Repulsive fermions in optical lattices: Phase separation versus coexistence of antiferromagnetism and d-wave superfluidity

S. Y. Chang, S. Pathak, and N. Trivedi

Repulsive Fermions in Optical Lattices: Phase separation versus Coexistence of Antiferromagnetism and d-Superfluidity

S. Y. Chang[1,2,5], S. Pathak[3,4], and N. Trivedi[5]

[1]*Institute for Theoretical Physics, University of Innsbruck, Technikerstr. 25, A-6020 Innsbruck Austria*
[2]*Institute for Quantum Optics and Quantum Information of the Austrian Academy of Sciences,*
ICT-Gebäude, Technikerstr. 21a, A-6020 Innsbruck Austria
[3]*Department of Physics, Louisiana State University,*
80 Nicholson Hall, Tower Dr., Baton Rouge, LA 70803, USA
[4]*Materials Research Center, Indian Institute of Science, Bangalore 560 012, India and*
[5]*Department of Physics, The Ohio State University,*
191 W. Woodruff Avenue, Columbus, Ohio 43210, USA

We investigate a system of fermions on a two-dimensional optical square lattice in the strongly repulsive coupling regime. In this case, the interactions can be controlled by laser intensity as well as by Feshbach resonance. We compare the energetics of states with resonating valence bond d-wave superfluidity, antiferromagnetic long range order and a homogeneous state with coexistence of superfluidity and antiferromagnetism. Using a variational formalism, we show that the energy density of a hole $e_{hole}(x)$ has a minimum at doping $x = x_c$ that signals phase separation between the antiferromagnetic and d-wave paired superfluid phases. The energy of the phase-separated ground state is however found to be very close to that of a homogeneous state with coexisting antiferromagnetic and superfluid orders. We explore the dependence of the energy on the interaction strength and on the three-site hopping terms and compare with the nearest neighbor hopping t-J model.

I. INTRODUCTION

The basic mechanism by which attractively interacting fermions can undergo Bardeen-Cooper-Schrieffer(BCS)-type transition through s-wave pairing is now well understood. The copper-oxide (CuO_2) materials are the first example of superconductivity arising from strong repulsive interactions [1]. It is argued that the single-band Hubbard model captures the essential physics of on-site repulsion. From variational calculations of the Hubbard model, the mechanism is now understood to be an antiferromagnetic exchange mechanism that favors singlet pairs on different sites leading to pairing in the d-wave channel [2]. These calculations show a strong deviation from the standard BCS paradigm with a separation of energy scales for pairing and long range coherence [3, 4]. However, in the absence of a rigorous solution of the Hubbard model in two dimensions, the nature of the ground state, and in particular, whether it is a d-wave superconductor or not is still in debate [5].

Given the difficulties of solving the Hubbard model, another route that is being currently attempted is to turn to the ultracold atoms in optical lattices [6, 7] and use them to emulate Hubbard-like models long studied in the condensed matter physics. Unlike the materials studied in the condensed matter physics in which the interaction strengths are usually fixed, in optical lattices the interactions can be varied over a wide range from weak to strong coupling. Furthermore, in the condensed matter systems changing carrier concentration usually modifies the degree of disorder, while the optical lattices are perfect and clean. Thus, the optical lattices allow direct simulation of one quantum system by another [8]. It is hoped that a deeper understanding of superconductivity in repulsive models will suggest mechanisms for driving the transition temperature higher. At present the main bottlenecks faced in creating low entropy states in optical lattices pertain to cooling mechanisms and the role of inhomogeneity introduced by an overall trapping potential. Also, the multi-band effects when strongly interacting fermions are loaded in the optical lattice, have to be carefully taken into account [9, 10].

In this article we discuss the problem of repulsively interacting fermions in a square optical lattice. The repulsion can be varied either by increasing the laser intensity or by Feshbach resonance. For both cases we derive an effective Hamiltonian in the strong coupling regime that is independent of the interaction mechanism. We expect both d-wave superconducting and antiferromagnetic fluctuations to dominate in the ground state. The main question we ask is whether the ground state energetically chooses to phase separate or to stay in a homogeneous state as doping and interactions are changed. In the past, analogous questions were addressed in perovskite compounds such as manganites [11–13]. In that case, the phase separation between undoped antiferromagnetic and hole-doped ferromagnetic regions was observed. The origin of the interaction was, however, coulombic repulsion between the localized and mobile electrons.

Our result is that fermions in the optical lattice show a tendency to phase separate at low hole density. This result is based on a variational theory that compares the energetics for two possible ground states: one that allows phase separation and another with homogeneous coexistence. Given the small difference in energy between the two solutions for phase separation and homogeneous coexistence, other factors may determine the ultimate behavior of the system: for example, long-range interactions may tend to favor coexistence whereas disorder may drive the system toward phase separation. Also, the effect of trapping potential needs to be better understood [14, 15].

II. MODEL

A. Hamiltonian

The interactions between fermions in the optical lattices can be controlled in two ways [16, 17]:

i) Laser Intensity controlled: By varying the laser intensity or the optical lattice depth V_o, we can modify the tunneling rate t of atoms between neighboring sites and the on-site interaction U. t and U can be calculated from the band structure theory. In the deep lattice limit, the tunneling rate is given by $t \approx \frac{4}{\sqrt{\pi}} E_r \left(\frac{V_o}{E_r} \right)^{3/4} \exp \left[-2 \left(\frac{V_o}{E_r} \right)^{1/2} \right]$ and the on-site interaction $U \approx \sqrt{\frac{8}{\pi}} a k_F E_r \left(\frac{V_o}{E_r} \right)^{3/4}$ [16], where a is the s-wave scattering length that is fixed and k_F is the Fermi wave vector. For realizing repulsive fermions, potassium isotope ^{40}K can be used where a for its hyperfine states is positive ($\approx 160 a_o$ [18]) with a_o defined as Bohr radius. Typical a for ^{6}Li is $\approx -2000 a_o$. Here $E_r = \frac{h^2}{2m\lambda^2}$ is the recoil energy of the optical lattice generated by a set of counter-propagating laser beams of wavelength λ. The expressions above are valid in the non-resonant regime where $k_F a \ll 1$. It is then possible to restrict the Hilbert space to a single band Hubbard model given by

$$\mathcal{H} = -t \sum_{<i,j>\sigma} c^\dagger_{i,\sigma} c_{j,\sigma} + U \sum_i n_{i,+1} n_{i,-1} \qquad (1)$$

where $\sigma = \pm 1$ is the *pseudo-spin* index. The sums $\langle i,j \rangle$ run over all pairs of nearest-neighbor lattice sites and $n_{i,\sigma} \equiv c^\dagger_{i,\sigma} c_{i,\sigma}$. We define doping parameter $x = 1 - N/N_{latt}$ where N is the total number of fermions of both spin species and N_{latt} is the number of sites in the optical lattice.

ii) Feshbach resonance controlled: This is by tuning the scattering length a using a magnetic field B. Scattering length near resonance takes the form $a = a_{bg}[1 - \Delta B/(B - B_o)]$ where a_{bg} is the background scattering length ($\approx 160 a_o$ for ^{40}K). Also $\Delta B \approx 8$G and $B_o \approx 202$ G for ^{40}K. Here, the scattering length a can be tuned from the positive values(repulsive) to zero(non-interacting) and to the negative values(attractive). Near the resonance, the interactions can be easily driven into a regime where they exceed the band gap or the energy difference between the lowest two levels in a single lattice site. In this resonant limit the wave function of the two-particle state includes contributions from all excited states and does not reduce to a symmetrized product of the two single particle ground state wave functions. Thus, the minimal set of basis per site should include a single particle ground state as well as a state with double occupancy. Consequently, the overlap of the wave functions for nearest neighbor sites and the hopping amplitudes depend on the particular configuration. This situation is illustrated in the Fig. 1. The physics of the resonant two-particle states introduces two additional parameters δt and δg, which are incorporated into the Hamiltonian in the following form [19, 20]

$$\mathcal{H} = - \sum_{<i,j>\sigma} [t + \delta g(n_{i,\bar\sigma} + n_{j,\bar\sigma}) + \delta t(n_{i,\bar\sigma} n_{j,\bar\sigma})] c^\dagger_{i,\sigma} c_{j,\sigma}$$
$$+ U_o \sum_i n_{i,+1} n_{i,-1}. \qquad (2)$$

Here, t is controlled by the optical lattice depth V_o as in Eq. 1. However in the Feshbach resonance case, not just the optical lattice depth V_o but also the applied magnetic field and other physical parameters of the system determine the value of U_o. Further discussions below and in the Appendix show that within second order perturbative theory, the Hamiltonians of Eq. 1 and Eq. 2 become analogous with the identification of an *effective* coupling U.

B. Our Approach

Given the Hamiltonian, the next step is to determine the quantum phases arising from the strongly repulsive interactions among fermions in two dimensions. At half filling, or zero doping ($x = 0$), the system is a Mott insulator with a finite gap in the charge spectrum and has long range antiferromagnetic order. As the system is doped with holes, antiferromagnetic order decreases and the system develops superfluidity described by a coherent superposition of the resonating valence bond (RVB) singlets [1]. Here, each singlet is formed by a pair of opposite fermion species in an orbital state with d-wave spatial symmetry. The question that arises is: What are
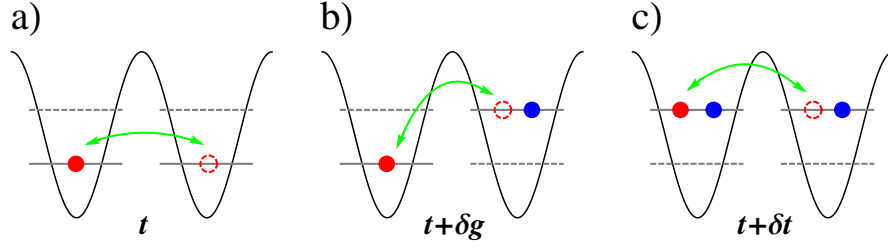
FIG. 1: (Color online) Here, we illustrate the effect of having a resonant two-particle state away from the single particle ground state. The hopping amplitudes are essentially given as the overlap of the wave functions of the neighboring sites. Thus, within this "two level" model we can identify three different hopping processes and amplitudes, a) from a single particle state to another single particle state, b) from a two-particle state to a single particle state or the reverse process, and c) from a two-particle state to another two-particle state. Blue and red colors indicate fermions with opposite spins.

the characteristics of the quantum phase at small hole density x?

In this article, we discuss two possible scenarios:

1) Phase Separation: In this scenario, the system is macroscopically phase separated into regions of antiferromagnetism and superfluidity. We calculate the behavior of the energy density of a hole $e_{hole}(x)$ to check for phase separation.

2) Homogeneous: Here, we consider a single homogeneous phase with coexisting antiferromagnetic and superfluid orders occupying the whole system. We evaluate the energetics of variational states that include both superfluid and antiferromagnetic orders.

By comparing with the more restricted standard t-J model we find that the presence of effective 3-site hopping terms in the *full* Hamiltonian defined in Eq. 4 leads, as we will see, to the lowering of energy at non-zero hole density x.

C. Effective Hamiltonian in Strong Coupling

In the large U/t limit, the Hamiltonian in Eq. 1 can be transformed into a block diagonal form where the blocks preserve the total number of the doubly occupied sites. Here, different blocks are connected by the kinetic/hopping operators (see Appendix). The effective Hamiltonian $\mathcal{H}_{eff}$ in the strong coupling limit is obtained by a canonical transformation[21, 22]

$$\mathcal{H}_{eff} = \mathcal{V} + \mathcal{K}_0 + \frac{1}{U}[\mathcal{K}_1, \mathcal{K}_{-1}] + \mathcal{O}(1/U^2) \qquad (3)$$

where the kinetic operator $\mathcal{K}_m$ changes the number of doubly occupied sites by an integer number m. $\mathcal{V}$ is the interaction term. The term given by the commutator (second order term) in Eq. 3 contains two consecutive hoppings. Since we consider $U/t >> 0$, we impose the non-double occupancy constraint at each site in order to obtain the low energy Hamiltonian: $\mathcal{H}_{eff} \to \mathcal{P}_G \mathcal{H}_{eff} \mathcal{P}_G$ where $\mathcal{P}_G = \prod_i (1 - n_{i,1} n_{i,2})$ is the *full* Gutzwiller projector. As a result, the interaction term $\mathcal{V}$ is projected out and the Hamiltonian can be cast as

$$\mathcal{H}_{eff} = -t \sum_{<i,j>\sigma} f_{i,\sigma}^\dagger f_{j,\sigma} - \frac{t^2}{U} \sum_{<i',i>\sigma';<i,j>\sigma} f_{i',\sigma'}^\dagger d_{i,\sigma'} d_{i,\sigma}^\dagger f_{j,\sigma} \qquad (4)$$

The summations run over all independent indices and Eq. 4 is what we call the *full* Hamiltonian to distinguish it from the more restricted t-J model. In the second sum, we can identify two-site (when $i' = j$) and three-site (when $i' \neq j$) processes. In the t-J model, an additional restriction $i' = j$ is imposed such that only two-site

exchange is allowed. In Figs. 6 and 7, we show the effects of this constraint. We have introduced definitions: $f_{i,\sigma}^\dagger \equiv h_{i,\bar\sigma} c_{i,\sigma}^\dagger$ the creation operator of a singly occupied site with spin σ particle and $d_{i,\sigma}^\dagger \equiv c_{i,\sigma}^\dagger h_{i,\sigma} n_{i,\bar\sigma}$ the creation operator of a doubly occupied site by adding a particle of spin σ to a singly occupied site with a

spin $\bar{\sigma}$ particle where $h_{i,\sigma} \equiv 1 - n_{i,\sigma}$. Rewriting the Hamiltonian in terms of the *pseudo-particle* operators $f_{i,\sigma}$, $f_{i,\sigma}^{\dagger}$, $d_{i,\sigma}$ and $d_{i,\sigma}^{\dagger}$ makes clear the permitted physical processes. However, these operators do not satisfy the usual anti-commutator nor commutator relations and straightforward theoretical treatment is difficult. Thus, we rely on the variational formalism whose accuracy depends on the chosen ansatz [23–25]. In the following section, we discuss the different variational wave functions.

For the fermions in the optical lattice near resonance (Eq. 2), the same perturbative Hamiltonian (Eq. 4) is derived with an *effective* interaction U which has two contributions

$$U = \frac{U_o}{(1 + \delta g/t)^2}. \qquad (5)$$

Here, U_o is controlled by the optical lattice depth and the magnetic field while $\delta g/t$ parameter accounts for the appearance of a two-particle state that goes beyond the single band model (see Appendix). The δg dependence comes from the allowed virtual processes while the δt terms do not appear in the second order perturbation. As a consequence, we now consider the phase diagram of the Hamiltonian in Eq. 4 as a function of U/t and doping x, regardless of the different ways of tuning the interaction U.

D. Variational Wave functions

1) Phase separated solution using Maxwell construction: Phase separation results from thermodynamic considerations that involve two pure phases. In the following, we give their description leaving the details of Maxwell construction to the section III (Discussion of Results).

The pure superfluid variational state is described by [4]

$$\begin{aligned}
|\Psi_{SF_d}\rangle &= \mathcal{J}\mathcal{P}_G\mathcal{P}_N|SF_d\rangle_{MF} \\
&= \mathcal{J}\mathcal{P}_G\left[\sum_{\mathbf{k}} \alpha_{\mathbf{k}} c_{\mathbf{k},\sigma}^{\dagger} c_{-\mathbf{k},\bar{\sigma}}^{\dagger}\right]^{N/2} |0\rangle
\end{aligned}$$
(6)

$|\Psi_{SF_d}\rangle$ is also called the RVB wave function when Jastrow correlation is set to unity. But as we discuss below, $|\Psi_{SF_d}\rangle$ is more general and can also describe a system with long range antiferromagnetism for an appropriate choice of the Jastrow correlations. $|SF_d\rangle_{MF}$ is

the solution of the simple mean field Hamiltonian of the form: $\mathcal{H}_{MF} = \sum_{\mathbf{k}\sigma} \xi_{\mathbf{k}} c_{\mathbf{k},\sigma}^{\dagger} c_{\mathbf{k},\sigma} + \sum_{\mathbf{k}} \Delta_{\mathbf{k}}[c_{\mathbf{k},+1}^{\dagger} c_{-\mathbf{k},-1}^{\dagger} + h.c.]$. Thus, the parameters $\alpha_{\mathbf{k}}$ are given as $\alpha_{\mathbf{k}} = \Delta_{\mathbf{k}}/\left[\xi_{\mathbf{k}} + \sqrt{\xi_{\mathbf{k}}^2 + \Delta_{\mathbf{k}}^2}\right]$. The d-wave parametrization $\Delta_{\mathbf{k}} = \Delta_d(\cos k_x - \cos k_y)$ is always energetically favorable in comparison with the s-wave symmetric parametrization. We get the appropriate μ_{var} from the number equation $N = \sum_{\mathbf{k}} \left[1 - \xi_{\mathbf{k}}/\sqrt{\xi_{\mathbf{k}}^2 + \Delta_{\mathbf{k}}^2}\right]$. Independent optimization of μ_{var} has a negligible effect on the energy. For our fully projected wave function of Eq. 6, we avoid attaching physical meanings to the parameters Δ_d and μ_{var}. They are taken simply as two independent degrees of freedom in the variational wave function. In order to characterize the quantum phases, the appropriate order parameters that characterize the SF and AF long range orders are calculated explicitly with the optimized wave functions. It can be seen that for the wave function of Ref. [26], when long range hopping parameters t' and t'' of $\xi_{\mathbf{k}}$ are set to zero, the $\alpha_{\mathbf{k}}$ parametrization of the wave function becomes equivalent to that of Ref. [27, 28] and Eq. 6. Unlike the case of high T_c materials where the t' and t'' terms are important to describe the correct band structure of the materials, in the context of cold atoms in optical lattices, these extra parameters can be set to zero.

The quantum phase at half filling (zero hole doping) has long range antiferromagnetic (AF) order [29]. For large enough system sizes, a broken SU(2) symmetric ground state becomes likely. In a ground state that has antiferromagnetic long range order, we note that even at zero doping, the singlet correlation accounts for large part of the energy contribution [30]. Thus, we keep the singlet correlation mechanism of Eq. 6 and adjust the fluctuations around the Neel state with a Jastrow factor that explicitly breaks the SU(2) symmetry: $\mathcal{J} = e^{m_{af}\Delta_{af}}$. Here,

$$m_{af} = \frac{2}{N_{latt}} \left[\sum_{i \in L_1} S_i^z - \sum_{i \in L_2} S_i^z\right] \qquad (7)$$

is the staggered magnetization operator with $S_i^z = 1/2(n_{i,+1} - n_{i,-1})$. Also, L_j is the sub-lattice of index j. Δ_{af} can be interpreted as a local magnetic field that breaks the SU(2) symmetry. Thus, for the zero doping case we are assuming three variational parameters: Δ_d, Δ_{af}, and μ_{var}. The improvement in energy due to the choice of the Jastrow factor $\mathcal{J} = e^{m_{af}\Delta_{af}}$ discussed above is $\sim 2\%$ compared to just setting $\mathcal{J} = 1$. This improvement is significantly larger than the typical statistical errors. It was found that the optimum value $\Delta_{af} \approx 0.35$ not only produces lower energy but also the correct staggered magnetization [29].

2) Homogeneous solution with coexistence of

antiferromagnetism and superfluidity: A homogeneous state with both the d-wave superfluid and staggered magnetic long range order(denoted by $|AF+SF_d\rangle$) is based on the mean field solution [26–28, 31, 32]. This state is favorable close to the zero hole doping $x = 0$ up to a critical $x = x_c$. While for $x_c \leq x \leq x'_c$, a pure d-wave superfluid (SF$_d$) phase is favored. The initial mean field $|AF+SF_d\rangle_{MF}$ state is obtained by solving the Hamiltonian

$$\mathcal{H}_{MF} = \sum_{\mathbf{k}\sigma}[\xi_{\mathbf{k}}c^{\dagger}_{\mathbf{k},\sigma}c_{\mathbf{k},\sigma} + \xi_{\mathbf{k}+\mathbf{Q}}c^{\dagger}_{\mathbf{k}+\mathbf{Q},\sigma}c_{\mathbf{k}+\mathbf{Q},\sigma}] + \sum_{\mathbf{k}}\{\Delta_{\mathbf{k}}[c^{\dagger}_{\mathbf{k},1}c^{\dagger}_{-\mathbf{k},-1} + h.c.] + \Delta_{\mathbf{k}+\mathbf{Q}}[c^{\dagger}_{\mathbf{k}+\mathbf{Q},1}c^{\dagger}_{-(\mathbf{k}+\mathbf{Q}),-1} + h.c.]\}$$
$$+ \frac{1}{4}\sum_{\mathbf{k}\sigma}\sigma m_N(\mathbf{Q})[c^{\dagger}_{\mathbf{k}+\mathbf{Q},\sigma}c_{\mathbf{k},\sigma} + c^{\dagger}_{\mathbf{k},\sigma}c_{\mathbf{k}+\mathbf{Q},\sigma}] \tag{8}$$

where the $\mathbf{k}$ vector is restricted to the *reduced Brillouin zone* and $\mathbf{Q} = (\pi, \pi)$. The diagonalization produces two spin density wave bands denoted by subindices a and b. The dispersion relations are given as

$$E_a(\mathbf{k}) = \frac{\xi_{\mathbf{k}} + \xi_{\mathbf{k}+\mathbf{Q}} + \sqrt{(\xi_{\mathbf{k}} - \xi_{\mathbf{k}-\mathbf{Q}})^2 + m_N(\mathbf{Q})^2}}{2}$$

$$E_b(\mathbf{k}) = \frac{\xi_{\mathbf{k}} + \xi_{\mathbf{k}+\mathbf{Q}} - \sqrt{(\xi_{\mathbf{k}} - \xi_{\mathbf{k}-\mathbf{Q}})^2 + m_N(\mathbf{Q})^2}}{2} \tag{9}$$

with $\xi_{\mathbf{k}} = -2t(cos(k_x) + cos(k_y)) - \mu_{var}$ and $m_N(\mathbf{Q}) = $ magnetic variational parameter. The corresponding quasiparticle operators are

$$d_{\mathbf{k},a,\sigma} = \alpha_{\mathbf{k}}c_{\mathbf{k},\sigma} + \sigma\beta_{\mathbf{k}}c_{\mathbf{k}+\mathbf{Q},\sigma}$$
$$d_{\mathbf{k},b,\sigma} = -\sigma\beta_{\mathbf{k}}c_{\mathbf{k},\sigma} + \alpha_{\mathbf{k}}c_{\mathbf{k}+\mathbf{Q},\sigma}. \tag{10}$$

From these, the ground state ansatz can be written as

$$|\Psi_{AF+SF_d}\rangle = \mathcal{J}\mathcal{P}_G\mathcal{P}_N|AF+SF_d\rangle_{MF} = \mathcal{J}\mathcal{P}_G\left[\sum_{\mathbf{k}}A_{\mathbf{k}}d^{\dagger}_{\mathbf{k},a,+1}d^{\dagger}_{-\mathbf{k},a,-1} + B_{\mathbf{k}}d^{\dagger}_{\mathbf{k},b,+1}d^{\dagger}_{-\mathbf{k},b,-1}\right]^{N/2}|0\rangle. \tag{11}$$

Here, $A_{\mathbf{k}} = \Delta_{\mathbf{k}}/\left[E_a(\mathbf{k}) + \sqrt{(E_a(\mathbf{k}))^2 + \Delta_{\mathbf{k}}^2}\right]$ and $B_{\mathbf{k}} = -\Delta_{\mathbf{k}}/\left[E_b(\mathbf{k}) + \sqrt{(E_b(\mathbf{k}))^2 + \Delta_{\mathbf{k}}^2}\right]$ with d-wave symmetric parametrization $\Delta_{\mathbf{k}} = \Delta_d(cos(k_x) - cos(k_y))/2$. $\mathcal{P}_N$ projects the wave function into the subspace of total number of particles $N = N_1 + N_2$ with equal populations $N_1 = N_2$. For this variational wave function, the optimization parameters are Δ_d, $m_N(\mathbf{Q})$, and μ_{var}.

In the hole doped regime, the contribution from particle-particle correlations is small and the hole-hole correlations dominate [25]. We assume a Jastrow factor $\mathcal{J}$ of the form $\mathcal{J} = e^{1/2\sum_{i,j}h_ih_jv_{ij}}$ where the hole density at *i-th* site is $h_i \equiv h_{i,1}h_{i,-1}$ and the correlation function is parametrized by $v_{ij} = v/|\mathbf{r}_i - \mathbf{r}_j|$. We find an improvement in energy of the order $\sim 0.1\%$ with $v < 0$ when compared to the case of setting $\mathcal{J} = 1$. Here, the distance between sites $r_{ij} = |\mathbf{r}_i - \mathbf{r}_j|$ must be between the closest images across the tilted boundaries as we later discuss.

III. DISCUSSION OF RESULTS

In analogy with the high T_c materials, we consider U values in the Eq. 4 centered at 13.33 (in units of t). For the case of the simple single band model (Eq. 1) this U value is solely controlled by the optical lattice depth V_o while for the model of Eq. 2, U is controlled by V_o as well as by Feshbach resonance(magnetic field). For our discussion, we assume the parametrization of Eq. 5 with $U_o = 13.33$ and $\delta g/t$ varied. For the non-resonant case, this is just a way of getting different values of U, while for the resonant case $\delta g/t$ has physical meaning. Our results

are summarized in the figures 2 - 8. The errors are either clearly marked with the data points or smaller than the size of the symbols when mentioned in the captions.

The quantum expectation values are evaluated by Monte Carlo multi-dimensional integration. In order to avoid numerical instabilities along the $k_x = k_y$ points, we take a patch of lattice sites with the tilted boundary conditions as our system frame [4, 33]. The size of the system is $N_{latt} = L^2 + 1$ sites, where L is an odd number. In this way, we also avoid the frustration of the antiferromagnetic phase (one particle of spin +1(-1) should be surrounded by 4 particles of spin -1(+1)) at the half filling density. The pairing wave function in real space is obtained by Fourier transforming α_k (Eq. 6). This pairing function is continuous when crossing the tilted boundaries. Since the variational wave functions used here depend only on a few parameters, we can find their optimal values by explicitly exploring the parameter space on a grid. For a larger number of parameters it will be useful to use a more powerful optimization method such as conjugate gradient method [34].

The injection of holes to the antiferromagnetic(AF) phase at half filling destabilizes the AF order. Beyond a critical hole doping density x_c, the AF order is completely destroyed giving way to the homogeneous d-wave superfluid (SF_d) (Eq. 6). There are two possible scenarios of AF $\leftrightarrow$ SF_d transitions considered here: 1) a first order phase transition between AF and SF_d phases as a function of doping. 2) a second order phase transition from a homogeneous $AF + SF_d$ phase at low doping densities to the SF_d phase. The energetics of this scenario is calculated using the wave function of Eq. 11. In both cases, the pure SF_d phase exists in the hole doping regime $x_c < x < x'_c$. For $x > x'_c$, the system becomes a normal Fermi fluid (NFF) phase with none of the long range antiferromagnetic and superfluid correlations. In all cases, the s-wave symmetric superfluidity is energetically disfavored.

A. Magnetic and Superfluid order parameters

In order to characterize the quantum phases, we calculate the following long range orders; d-wave order $\Phi = \lim_{j \to \infty} \phi(j)$. Here, we defined $\phi(j) \equiv \sqrt{2/N \langle \sum_i B^\dagger_{i+j\hat{x}} B_{i\hat{y}} \rangle}$ with $B^\dagger_{i\alpha} \equiv 1/2(c^\dagger_{i,+1} c^\dagger_{i+\alpha,-1} - c^\dagger_{i,-1} c^\dagger_{i+\alpha,+1})$. And the long range order for the staggered magnetization $M_{AF} = \langle m_{af} \rangle$ (Eq. 7). As shown in the Fig. 2, Φ has a region of favorable d-wave paring at finite hole densities. At zero hole density, we found that the broken SU(2)
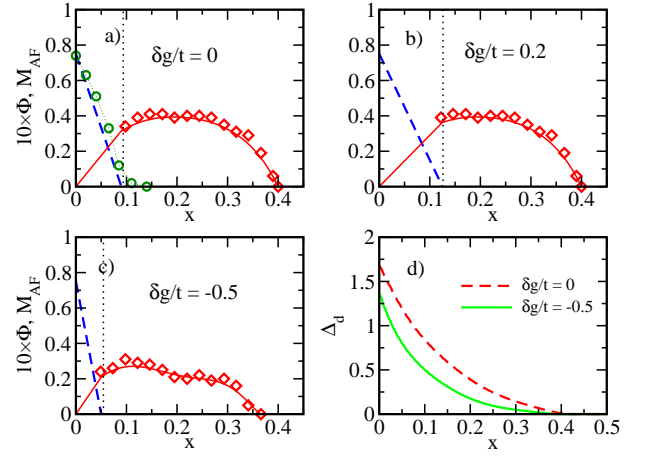

FIG. 2: (Color online) Superfluid long range order Φ (diamonds, continuous line) and antiferromagnetic order parameter M_{AF} (dashed line) at different hole densities and coupling U (plots a-c). These figures correspond to the scenario with phase separation. Here, we assumed the *full* Hamiltonian of Eq. 4 and the interaction parametrized by $U = U_o/(1+\delta g/t)^2$ with $U_o = 13.33$ in units of t (Eq. 5). In the phase separated region $0 < x < x_c$ (vertical dotted line), the order parameters are assumed to depend linearly on x, so that $\Phi(x) = \Phi(x_c)x/x_c$ and $M_{AF}(x) = M_{AF}(0)[1 - x/x_c]$. For comparison, we also show $M_{AF}(x)$ for the homogeneous phase scenario(circles) at the interaction given by $\delta g/t = 0$ (plot a). There is a distinguishable difference for the optimizing superfluid parameter Δ_d between $\delta g/t = 0$ and $\delta g/t = -0.5$ (plot d). However, there is only a small difference for Δ_d between $\delta g/t = 0$ and $\delta g/t = 0.2$ cases; thus we use the same parametrization for both. The optimum value of the antiferromagnetic parameter Δ_{af} was ~ 0.35 at $x = 0$. It has a rather weak dependence on $\delta g/t$ (that is, on U). As we remark later (see the caption of Fig. 3), the location of the critical doping x_c for $\delta g/t = -0.5$ (plot c) is more affected by finite size corrections compared to the weaker coupling cases.

symmetry wave function produces the correct finite size behavior of $M_{AF} = 0.75(2)$ in agreement with previous variational calculations [26, 29] for the considered system sizes ($N_{latt} = 50$ to 226). These long range orders, however, cannot provide information on the nature of the phase transition (first or second order). In fact, we find that the order parameters for the phase separation scenario and the homogeneous phase scenario are very close to each other in values.

B. Phase separation vs Coexistence at low hole doping

In order to characterize the inhomogeneous mixture phase, the thermodynamic considerations are as following: From thermodynamic constraints, the energy per
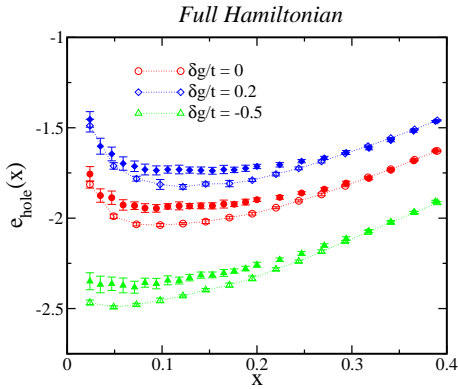
FIG. 3: (Color online) Energy density per hole $e_{hole}(x)$ as a function of the hole density x is shown for the *full* Hamiltonian model. The interaction strengths corresponding to $\delta g/t = -0.5$ ($U/t = 53.32$), 0 ($U/t = U_o/t = 13.33$) and 0.2 ($U/t = 9.26$) cases are considered. The results are for $N_{latt} = 82$ (empty symbols) and 170 (full symbols) lattice sites. We notice that with the increased system size, $e_{hole}(x)$ becomes flatter around the x_c. However, we observe that $e_{hole}(x)$ for $\delta g/t = 0$ and $= 0.2$ continues to show a distinct minimum at $x_c > 0$ signaling phase separation in the region $0 < x < x_c$. On the other hand, for $\delta g/t = -0.5$, the mixed phase could be *washed out* in the thermodynamic limit. Thus the tendency for the system to phase separate is reduced at large values of U. The unit of energy is t.

site of the ground state $\mathcal{E}(x) = E(x)/N_{latt}$ has to be a convex function $\partial^2\mathcal{E}(x)/\partial x^2 \geq 0$. The range of $x \in (x_0, x_1)$ where $\partial\mathcal{E}(x)/\partial x = constant$ (or $\partial^2\mathcal{E}(x)/\partial x^2 = 0$) implies that the number of holes can be varied while the chemical potential $\mu = \partial\mathcal{E}(x)/\partial x$ is kept the same. This is a signature of the first order phase transition. In this regime, the system is a mixture of phase I at x_0 and phase II at x_1. In our case, $x_0 = 0$ and phase I has antiferromagnetic order(AF) while $x_c \equiv x_1$ and phase II is the d-wave superfluid(SF_d). In order to check whether there is an interval defined by $x = 0$ and $x_c > 0$, we should check for the *straightness* of $\mathcal{E}(x)$ [35]. However, because *we lack the knowledge of the exact mixed phase ground state at all x* we use the Maxwell construction: we calculate the energy per hole $e_{hole}(x)$ and check for the existence of the minimum[36] of

$$e_{hole}(x) = \frac{\mathcal{E}_{II}(x) - \mathcal{E}_I(0)}{x}, \qquad (12)$$

where $\mathcal{E}_{I,II}(x)$ are the energy densities of the pure phases (AF and SF_d). This is equivalent to finding x_c such that $\frac{\partial\mathcal{E}_{II}(x)}{\partial x}\big|_{x_c} = \frac{\mathcal{E}_{II}(x_c) - \mathcal{E}_I(0)}{x_c}$. For the cases with $\delta g/t = 0$ and $\delta g/t = 0.2$, $e_{hole}(x)$ can clearly have minimum (Fig. 3) and Maxwell construction with non zero x_c is possible. In order to avoid pair breaking effects, we introduce two holes at a time by removing one particle of each species. From Fig. 3, we find that the critical doping strengths are: for $\delta g/t = 0$, $x_c \approx 0.09$, for $\delta g/t = 0.2$, $x_c \approx 0.12$, and for $\delta g/t = -0.5$, $x_c \sim 0.05$ (true for $L = 9$. However for $L \gtrsim 13$, x_c is not well defined. See Fig. 3).

Correspondingly, the long range orders within the region $0 < x < x_c$ are proportional to the areas of the pure quantum phases; that is, the AF phase with $x = 0$ and SF_d phase with $x = x_c$ (see the caption of Fig. 2). The tendency is that smaller U is more favorable for d-wave superfludity with a larger mixed phase region (Fig. 2 and 3).

Regarding the status of phase separation in the literature, the reports have been rather controversial. Initial VMC calculations on the *t-J* model found indications of phase separation [37] that were later refuted by more accurate Green's Function Monte Carlo (GFMC) calculations [37, 38] in which strong size dependence was found. According to these GFMC analyses for large enough lattice size and $J/t \lesssim 0.7$ (or $U/t \gtrsim 5.7$ by taking $U/t = 4t/J$), the mixed phase would be unfavorable while in the regime $J/t \gtrsim 0.7$ (or $U/t \lesssim 5.7$) the mixed phase appears to be more robust. However, more recent works [39] using constrained path integral QMC for the Hubbard model at various values of $U/t(= 2, 4, 6, 8)$ and system sizes ($N_{latt} = 64 \sim 256$) and also simulations of the *t-J* model using projected entangled pair states (PEPS) [40] found very clear signatures of phase separation.

Our results are consistent qualitatively with the findings of the above mentioned references that there are clear indications of phase separation at weak to intermediate coupling. The phase separation becomes ambiguous as interaction is turned up. However, we differ quantitatively on the values of the interaction that show phase separation due to the differences in the model and the formalism.

C. Ground State Energies

The ground state energies for the *full* Hamiltonian are shown in the Fig. 4. We notice that the mixed phase and the homogeneous phase energies are closely degenerate within the region of $x \in (0, x_c)$ in all of the considered cases. The kinetic energy has no contribution at zero doping. In this case, the only contribution comes from the exchange. As holes are injected to the system, exchange of particles becomes suppressed while the kinetic contribution increases. In the normal phase regime beyond x'_c, most of the contribution to the energy comes from the kinetic terms. The composition of energies for the *t-J* model is shown in the Fig. 8.

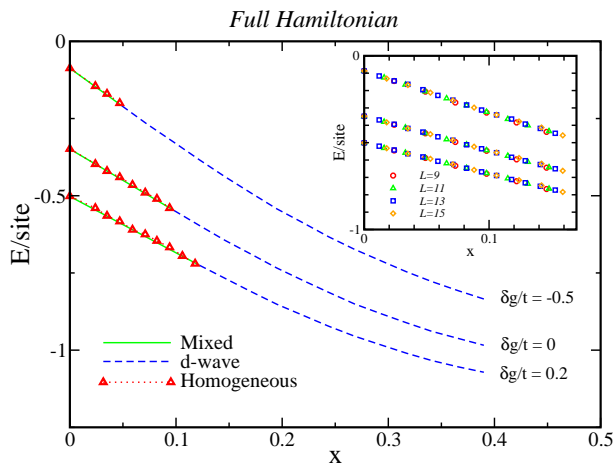From the Fig. 5, we see a monotonically decreasing be-

FIG. 4: (Color online) The ground state energies of Hamiltonian in Eq. 4 as a function of doping x for various interaction strengths parametrized by $\delta g/t$: $\delta g/t = -0.5$ ($U/t = 53.32$), 0 ($U/t = U_o/t = 13.33$) and 0.2 ($U/t = 9.26$). Within the region defined by $x \in (0, x_c)$, we also show the energies corresponding to the first order (continuous line) and the second order (triangle) phase transition scenarios. The energies are shown to be degenerate (within the error bars) for the mixed and the homogeneous cases. SF_d smoothly transitions to the normal Fermi fluid NFF at $x \gtrsim x'_c$ ($x'_c \approx 0.4$) when $\Delta_d \to 0$. These data are for 170 lattice sites. The statistical errors are smaller than the size of the symbols. The inset figure shows the ground state energy of the homogeneous phase for different system sizes. The unit of energy is t.
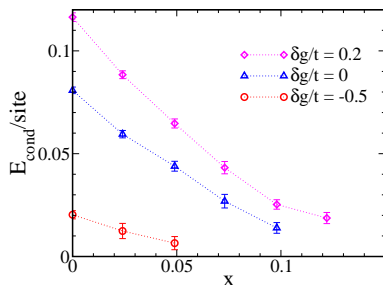

FIG. 5: (Color online) Condensation energy per site at different values of $\delta g/t$ for the Hamiltonian of Eq. 4. Hole densities x between 0 and x_c are considered. In this case, $x = 0$ corresponds to the pure antiferromagnet while $x = x_c$ corresponds to the pure superfluid phase. For $0 < x < x_c$, the condensation energy is that of the homogeneous solution. The unit of energy is t.

havior of the condensation energy E_{cond} which is the difference in energies between the normal state and the state with quantum coherence. Since E_{cond} is at its largest for the pure antiferromagnetic phase, we can argue that once the system is phase separated it would not transition into the homogeneous phase. This would be true even when the superfluid portion of the system is destroyed by thermal fluctuations as long as the antiferromagnetic portion retains its phase coherence. Thus, we argue that the phase separation scenario is more *robust* than the homo-

geneous coexistence.

D. Comparison of the *Full* vs t-J models

In the Figs. 6 and 7, a comparison of the *full* and the t-J Hamiltonians at different values of $\delta g/t$ is given. Both models converge at the zero doping $x = 0$ since three-site hopping terms are density suppressed. However, at finite doping, differences arise. Although for smaller system size $e_{hole}(x)$ of the *full* model tends to have a slightly larger curvature leading to a clear definition of x_c, this feature disappears in the thermodynamic limit. The location of x_c is better defined for smaller U. However, for $U << U_o$ the validity of the perturbative Hamiltonian (Eq. 3 and 4) is being compromised. The values of x_c seem to be identical within the errors for these two models; t-J and *full*.

IV. CONCLUDING REMARKS

We have investigated the appearance of different quantum phases in a system of strongly interacting fermions in the two dimensional optical lattices. We have shown the phase diagram that can be obtained by tuning the Feshbach resonance and by controlling the depth of the optical lattice. We found similar qualitative features as in the t-J [37, 38, 40] and Hubbard [39] models although quantitatively the interaction strengths may differ.

In the laboratory, the optical lattice is usually placed within a smoothly varying harmonic trap. Then, the usual shell structure is expected to appear. We have shown that the mixed phase is energetically allowed and possibly more robust than the homogeneous phase.

There are several experimental techniques to measure the quantum correlations: for example, radio frequency techniques to directly measure the excitation spectrum of the Fermi gas are being developed (see Ref. [41]). The measurement of the correlations in the noise could also be used, as it was applied to the detection of the Mott insulator phase (see Ref. [16]). Also, Bragg scattering is a scheme that allows the detection of the nodal points in the momentum space [42]. In the present work, a connection of the single band model to the resonant regime was made through perturbation theory, although a more elaborate multi-band model might be required for improved description.
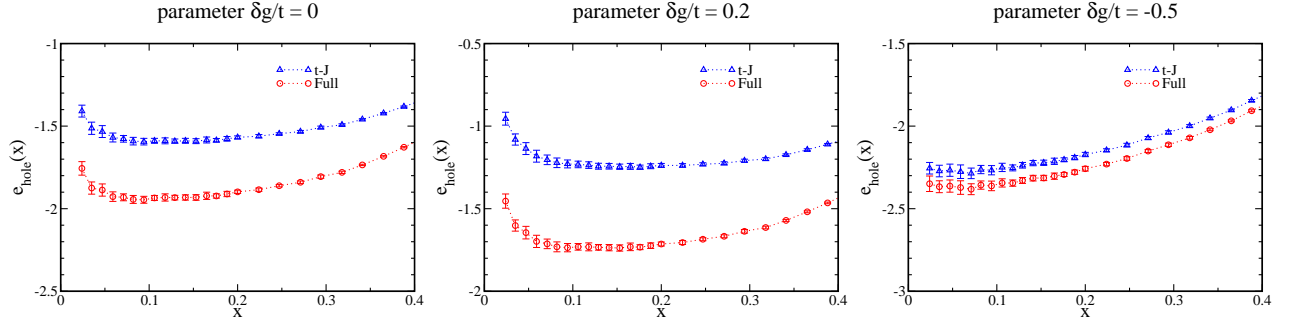
FIG. 6: (Color online) Comparison of the energy density per hole $e_{hole}(x)$ for the *full* and the *t-J* Hamiltonians at different values of $\delta g/t$: $\delta g/t = -0.5$ ($U/t = 53.32$), 0 ($U/t = U_o/t = 13.33$) and 0.2 ($U/t = 9.26$). The system is composed of 170 lattice sites. The unit of energy is t.
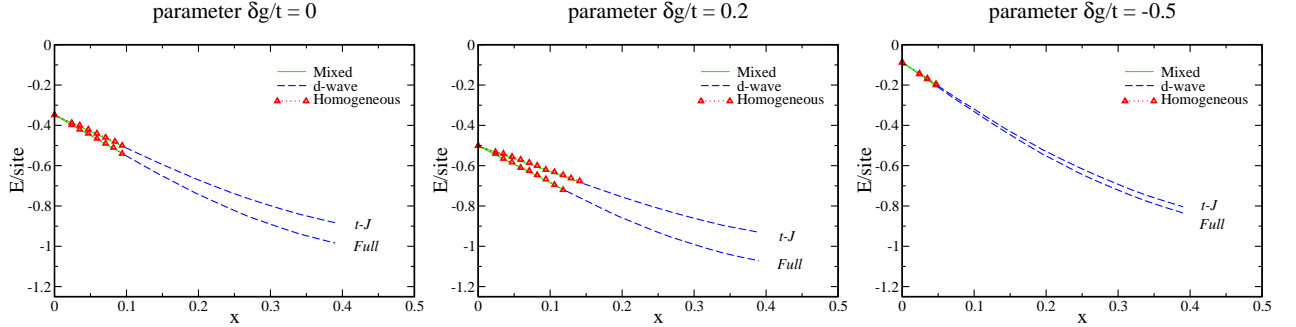

FIG. 7: (Color online) Comparison of the ground state energies for the *full* and the *t-J* Hamiltonians at different values of $\delta g/t$: $\delta g/t = -0.5$ ($U/t = 53.32$), 0 ($U/t = U_o/t = 13.33$) and 0.2 ($U/t = 9.26$). The *full* Hamiltonian includes three-site hopping terms (Eq. 4) that lower the energy relative to the *t-J* model. At zero hole doping, three-site terms are suppressed and both models converge. The unit of energy is t. Here, $N_{latt} = 170$. The statistical errors are smaller than the size of the symbols.
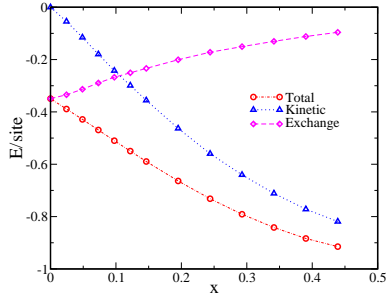

FIG. 8: (Color online) Doping dependence of the total, kinetic and exchange energies for the *t-J* model. The statistical errors are smaller than the size of the symbols. The unit of energy is t.

V.   APPENDIX

For the resonant fermions with large s-wave scattering length, multi-band effects have to be included. A model by Duan[19, 20] accounts them by an effective single-band Hubbard-type model. A heuristic argument for deriving this Hamiltonian is given in the following.

This approach physically corresponds to taking into account only the lowest energy but exact one-particle and two-particle states on each lattice site. For a single-particle state, the corresponding wave function is simply the ground sate wave function in the local potential well. In the strongly interacting limit, the wave function of a two-particle state includes contributions of all excited states and does not reduce to a properly symmetrized product of the two ground state wave functions. As a result, the overlap of the wave functions for nearest neighbor sites and, therefore, the hopping amplitude between them will depend on a particular density configuration (see Fig. 1): The hopping amplitude $t_{01} = t_{10} = t$ for the hop from a singly occupied site to an empty site, will be different from the hopping amplitudes

$t_{11} = t_{02} = t_{20} = t + \delta g$ for a hop from a singly occupied site to another singly occupied one and for a reverse hop from a doubly occupied site to an empty one, respectively. This is because the amplitude t_{01} contains the overlap between the two ground state wave functions on the nearest-neighbor sites, while the amplitudes $t_{11} = t_{02}$ are determined by the overlap of the exact two-particle wave function on a site with the product of the ground state wave functions on the same and the nearest-neighbor sites. In turn, the hopping amplitude $t_{12} = t_{21} = t + \delta t$ for a hop from a doubly occupied site to a singly occupied site contains the overlap of the exact two-particle wave functions on the nearest-neighbor sites. Hence, $t_{12} = t_{21}$ will be different from both t_{01} and $t_{11} = t_{02}$. As a result, the Hamiltonian of the extended Hubbard model reads

$$\mathcal{H} = -\sum_{<i,j>\sigma} [t + \delta g(n_{i,\bar{\sigma}} + n_{j,\bar{\sigma}}) + \delta t(n_{i,\bar{\sigma}} n_{j,\bar{\sigma}})] c_{i,\sigma}^\dagger c_{j,\sigma}$$
$$+ U_o \sum_i n_{i,+1} n_{i,-1}, \qquad (13)$$

where the density assisted hopping terms in the kinetic energy is characterized by δg and δt.

The coefficients $\delta g/t$ and $\delta t/t$ depend on the characteristics of the atomic species such as the width (in magnetic field) of the resonance ΔB, the background scattering length a_{bg} and the difference of the atomic magnetic moments between the closed and the open scattering channels $\Delta \mu$. In particular, $\delta g/t$ can be written as $\delta g/t \approx (0.38(V_o/E_r)^{0.25} - 1) + \alpha$ (see the Fig. 1 of the Ref. [19]). α is a weakly dependent quantity of V_o/E_r and proportional to $\sqrt{\Delta B |a_{bg}| \Delta \mu}$. Thus, for a given

atomic species and a resonant magnetic field, $\delta g/t$ can be tuned over a range of the optical lattice depths.

We define the kinetic operators $\mathcal{K}_m$ as

$$\mathcal{K}_0 = -t \sum_{<i,j>\sigma} h_{i,\bar{\sigma}} c_{i,\sigma}^\dagger c_{j,\sigma} h_{j,\bar{\sigma}}$$
$$- (t + 2\delta g + \delta t) \sum_{<i,j>\sigma} n_{i,\bar{\sigma}} c_{i,\sigma}^\dagger c_{j,\sigma} n_{j,\bar{\sigma}}$$
$$\mathcal{K}_1 = -(t + \delta g) \sum_{<i,j>\sigma} n_{i,\bar{\sigma}} c_{i,\sigma}^\dagger c_{j,\sigma} h_{j,\bar{\sigma}}$$
$$\mathcal{K}_{-1} = -(t + \delta g) \sum_{<i,j>\sigma} h_{i,\bar{\sigma}} c_{i,\sigma}^\dagger c_{j,\sigma} n_{j,\bar{\sigma}} \qquad (14)$$

$\mathcal{K}_m$'s change the number of doubly occupied sites by m and obey commutation relation $[\mathcal{V}, \mathcal{K}_m] = m U_o \mathcal{K}_m$ where interaction potential $\mathcal{V} = U_o \sum_i n_{i,+1} n_{i,-1}$ is assumed.

Here, we have used the usual definition $h_{i,\sigma} \equiv 1 - n_{i,\sigma}$. The *full* Gutzwiller projector can be shown to drop the interaction and the δt dependent terms. The effective Hamiltonian after Schrieffer-Wolff transformation is then the same as Eq. 4 with the definition of the effective $U \equiv U_o/(1 + \delta g/t)^2$. In a recent work [43] on the one dimensional attractive fermionic gas with population imbalance, it was found that the pairing order gets enhanced with $\delta g < 0$, while the spin-spin correlation is suppressed. Obviously, due to the difference in the dimensionality (1D vs 2D) and the nature of the interaction (attractive vs repulsive), an intuitive connection is rather complicated.

[1] P. W. Anderson, Scence **235**, 1196 (1987).
[2] P. W. Anderson, P. A. Lee, M. Randeria, T. M. Rice, N. Trivedi, and F. C. Zhang, J. Phys. Cond. Mat. **16**, R755(2004).
[3] M. Randeria, N. Trivedi, A. Moreo, and R. T. Scalettar, Phys. Rev. Lett. **69**, 2001 (1992).
[4] A. Paramekanti, M. Randeria, and N. Trivedi, Phys. Rev. Lett. **87**, 217002 (2001). M. Randeria, A. Paramekanti, and N. Trivedi, Phys. Rev. B **69**, 144509 (2004).
[5] C. J. Jia, B. Moritz, C.-C. Chen, B. Sriram Shastry, and T. P. Devereaux, Phys. Rev. B **84**, 125113 (2011).
[6] D. Jaksch, C. Bruder, J. I. Cirac, C. W. Gardiner, and P. Zoller, Phys. Rev. Lett. **81**, 3108 (1998).
[7] M. Greiner, O. Mandel, T. Esslinger, T. W. Hänsch, and I. bloch, Nature **415**, 39 (2002).
[8] R. Feynman, Int. J. Theor. Phys. **21**, 467 (1982).
[9] R. B. Diener and T.-L. Ho, Phys. Rev. Lett. **96**, 010402 (2006)
[10] H. P. Büchler, Phys. Rev. Lett. **104**, 090402 (2010).
[11] S. Yunoki, J. Hu, A. L. Malvezzi, A. Moreo, N. Furukawa, and E. Dagotto, Phys. Rev. Lett. **80**, 845 (1998).
[12] A. Moreo, S. Yunoki, and E. Dagotto, Science **283**, 2034 (1999).
[13] E. Dagotto, *Nanoscale Phase Separation and Colossal Magnetoresistance: The Physics of Manganites and Related Compounds*, Springer-Verlag, Berlin Heidelberg (2010).
[14] Q. Zhou, Y. Kato, N. Kawashima, and N. Trivedi, Phys. Rev. Lett. **103**, 085701 (2009).
[15] K. W. Mahmud, E. N. Duchon, Y. Kato, N. Kawashima, R. T. Scalettar, and N. Trivedi, Phys. Rev. B **84**, 054302 (2011).
[16] I. Bloch, J. Dalibard, and W. Zwerger, Rev. of Mod. Phys. **80**, 885 (2008).
[17] U. Schneider, *PhD. Thesis*, Johannes Gutenberg University of Mainz (2010).
[18] R. Cote, A. Dalgarno, H. Wang, and W. C. Stwalley, Phys. Rev. A **57**, R4118 (1998).
[19] L.-M. Duan, Phys. Rev. Lett. **95**, 243202 (2005).
[20] L.-M. Duan, Europhysics Lett. **81**, 20001 (2008).
[21] A. H. MacDonald, S. M. Girvin, and D. Yoshioka, Phys. Rev. B **37**, 9753 (1988).

[22] C. Cohen-Tannoudji, J. Dupont-Roc, and G. Grynberg, *Atom-Photon Interactions*, John Wiley & Sons (1992).

[23] B. Edegger, V. N. Muthukumar, and C. Gros, Advances in Physics **56**, 927 (2007).

[24] B. Edegger, V. N. Muthukumar, C. Gros, and P. W. Anderson, Phys. Rev. Lett. **96**, 207002 (2006).

[25] S. Sorella, et al, Phys. Rev. Lett. **88**, 117002 (2002).

[26] S. Pathak, et al, Phys. Rev. Lett. **102**, 027002 (2009).

[27] T. Giamarchi and C. Lhullier, Phys. Rev. B **43**, 12943 (1990).

[28] A. Himeda and M. Ogata, Phys. Rev. B **60**, R9935 (1999).

[29] N. Trivedi and D. M. Ceperley, Phys. Rev. B **41**, 4552 (1990).

[30] S. Liang, B. Doucot, and P. W. Anderson, Phys. Rev. Lett. **61**, 365 (1988).

[31] T. Lee, and C. Shih, Phys. Rev. B **55**, 5983 (1997).

[32] T. Lee, C.-M. Ho, and N. Nagaosa, Phys. Rev. Lett. **90**, 067001 (2003).

[33] E. Kaxiras and E. Manousakis, Phys. Rev. B **37**, 656 (1988).

[34] W. H. Press, S. A. Teukolsky, W. T. Vetterling, and B. P. Flannery, *Numerical Recipes*, University Press, Cambridge (2007).

[35] M. Boninsegni and N. V. Prokof'ev, Phys. Rev. B **77**, 092502 (2008).

[36] V. J. Emery, S. A. Kivelson, and H. Q. Lin, Phys. Rev. Lett. **64**, 475 (1990).

[37] M. Calandra, F. Becca, and S. Sorella, Phys. Rev. Lett. **81**, 5185 (1998).

[38] M. Lugas, L. Spanu, F. Becca, and S. Sorella, Phys. Rev. B **74**, 165122 (2006).

[39] C.-C. Chang and S. zhang, Phys. Rev. B **78**, 165101 (2008).

[40] P. Corboz, S. R. White, G. Vidal, and M. Troyer, Phys. Rev. B **84**,041108 (2011).

[41] J. T. Stewart, J. P. Gaebler, and D. S. Jin, Nature **454**, 744 (2008).

[42] W. Hofstetter, J. I. Cirac, P. Zoller, E. Demler, and M. D. Lukin, Phys. Rev. Lett **89**, 220407 (2002).

[43] B. Wang and L.-M. Duan, Phys. Rev. A **79**, 043612 (2009).